Frame-Frequency Estimation in Ultrawideband Systems

Antonio A. D'Amico and Umberto Mengali, *Life Fellow, IEEE*

***Abstract*—This paper investigates the estimation of the frame frequency in ultrawideband (UWB) communication systems. An estimation method is proposed that exploits the transmission of a periodic pulse sequence at the frame frequency. The samples of the received waveform are used to compute a cost function that depends on a trial value of the incoming pulse frequency. The location of the maximum provides an estimate of the transmitted frequency. The performance of the estimator is assessed theoretically and is compared to the Cramer–Rao lower bound. It is shown that in certain conditions the estimator achieves the bound at high SNR values. Simulations validate the theory and show the degradations in the estimation performance caused by multiple-access interference. They also give an idea of the estimation accuracy needed in a correlation receiver.**

***Index Terms*—Frame-frequency estimation, least-squares method, synchronization, ultrawideband (UWB) communications.**

I. Introduction

ULTRAWIDEBAND (UWB) communications are currently the focus of intense research activity aiming at the exploitation of the vast unlicensed spectrum from 3.1 through 10.6 GHz made available by the Report and Order of the Federal Communications Commission (FCC). A promising technology in this area is impulse radio, in which the signal bandwidth is expanded by transmitting subnanosecond pulses. The interest for commercial applications of impulsive radio stems from many favorable features [1], [2]. First, signal echoes with differential delays of nanoseconds can be resolved and combined to take advantage of the multipath channel diversity. Secondly, the same transmission medium can be shared by hundreds of users. Finally, as UWB communications operate at very low power spectral densities, they can overlay traditional narrowband systems with limited interference. To realize these attractive features, however, some formidable technological problems must be addressed. These include: 1) high detector sensitivity to timing errors [3], [4]; 2) complexity of the receiver architectures [5]–[7] and of the channel-estimation algorithms [8]–[11]; 3) strict limitations on the emitted power to minimize the interference over existing services that already use the same spectrum [12], [13].

Manuscript received February 18, 2004; revised July 15, 2004; accepted September 17, 2004. The editor coordinating the review of this paper and approving it for publication is C. Tellambura. This paper was supported by the Italian Ministry of Education in the framework of the project Piattaforme Riconfigurabili per Interoperabilità in MObilità (PRIMO), Fondo per gli Investimenti della Ricerca di Base (FIRB) 2001.

The authors are with the Department of Information Engineering, University of Pisa, Pisa 56100, Italy (e-mail: antonio.damico@iet.unipi.it; umberto.mengali@iet.unipi.it).

Digital Object Identifier 10.1109/TWC.2005.858344

Intuitively, the sensitivity to timing arises from the extremely narrow pulses employed in impulse radio. Sampling errors as small as a fraction of a nanosecond markedly affect the receiver performance [3]. Even if less intuitive, the pulse shortness and the sparseness of the pulse replicas at the output of a multipath channel make channel estimation a challenging task [8], [14]. Further complications in synchronization and channel-estimation operations stem from the frequency instabilities in the transmit/receive clocks. In impulse radio, the information is conveyed by a pulse stream and a single data symbol is associated to N_f consecutive pulses, each located in a frame of T_f seconds. The ratio of T_f to the pulse duration T_p is on the order of 100 or more. Now, suppose that the frame length T_f at the transmitter is slightly different from that T_f' at the receiver (as a consequence of the thermal drifts of the oscillators). On the receiver time scale, which ticks at multiples of T_f', the arriving pulses are seen to drift leftward or rightward according to whether $T_f' \gtrless T_f$. Clearly, the drift undermines the data-detection process unless it is compensated.

To cope with this problem, two solutions are available [15], [16]: 1) feedforward synchronizers, in which the receiver clock is free running but the drift is periodically measured and accounted for in computing the decision statistic; 2) feedback synchronizers, in which the receiver clock is locked to the incoming pulse rate, meaning that the drift is continuously measured and updated. In traditional narrowband communications, both types of synchronizers are implemented with no particular requirements on the oscillator stabilities. Vice versa, as we shall see soon, in UWB systems, the requirements are rather stringent. To illustrate this point, we concentrate on feedforward schemes, but the essence of our arguments holds with feedback schemes as well.

The difficulty in measuring the drift arises from two conflicting constraints. On one side, the interval over which the measurement is performed must be sufficiently long to achieve a good accuracy. On the other, as is explained soon, it must be short enough so that the overall drift across the interval is small compared to the pulse duration. More precisely, suppose that the first condition is satisfied with an interval of N_s symbols and call

$$\theta = \frac{\left(T_f' - T_f\right)}{T_f} \tag{1}$$

the normalized drift per frame. As a symbol has N_f frames, the total drift over N_s symbols is $N_s N_f T_f \theta$ and this quantity must

be much smaller than T_p, i.e., the following condition must hold

$$\theta \ll \frac{T_p}{N_s N_f T_f}. \tag{2}$$

Before explaining why this is so, we point out the difference between narrowband and UWB systems in meeting (2). In the former, there is a single frame per symbol and its duration is comparable to the pulsewidth, i.e., $N_f = 1$ and $T_f \simeq T_p$. For example, for $N_s = 50$, from (2) we have $\theta \ll 2 \times 10^{-3}$, which is easily satisfied, even with low-cost oscillators. On the contrary in impulsive radio N_f may be a few tens and T_f/T_p is much greater than unity. For example, for $T_f/T_p = 100$, $N_f = 25$, and $N_s = 50$, we have $\theta \ll 8 \times 10^{-6}$, which is rather stringent if we bear in mind that θ is the sum of the frequency stabilities of the transmit and receive clocks and that, even with temperature-compensated crystal oscillators, such stabilities may be some parts per million.

To gain a physical insight into (2), suppose that a periodic train of pulses is transmitted

$$s(t) = \sum_{i=0}^{N-1} g(t - iT_f) \tag{3}$$

where $g(t)$ is a short pulse of duration $T_p < T_f$. The channel has a single path with unity gain and unknown delay $\tau \in [0, T_f)$ and the disturbance $v(t)$ is additive white Gaussian noise (AWGN). Thus, the received waveform is

$$r(t) = s(t - \tau) + v(t). \tag{4}$$

Assuming that $g(t)$ is known, we want to estimate τ, ignoring the mismatch between T_f' and T_f, i.e., taking T_f' as the true pulse-repetition period. Note that this scenario is simplified for illustration purposes. With a realistic UWB channel, the received signal corresponding to a single excitation pulse is the superposition of many distorted replicas of the pulse, each with its own amplitude and delay [17].

In Appendix A, it is shown that the maximum-likelihood estimate of τ is computed as follows. First, $r(t)$ is folded N times with period T_f' to form

$$r_{\rm fold}(t) = \frac{1}{N} \sum_{i=0}^{N-1} r\left(t + iT_f'\right). \tag{5}$$

Next, $r_{\rm fold}(t)$ is fed to the matched filter $g(-t)$ to compute the convolution $x(t) = r_{\rm fold}(t) * g(-t)$. Finally, the maximum of $x(t)$ is sought and its location provides the desired estimate.

The impact of θ on the estimation accuracy is qualitatively assessed from the shape of the noise-free component of $x(t)$ in the interval $[0, T_f)$. In Appendix A, it is shown that

$$x(t) = p(t - \tau) + n(t), \qquad t \in [0, T_f) \tag{6}$$

where $n(t)$ represents the noise contribution, while $p(t)$ is given by

$$p(t) = \frac{1}{N} \sum_{i=0}^{N-1} \gamma(t + i\theta T_f) \tag{7}$$

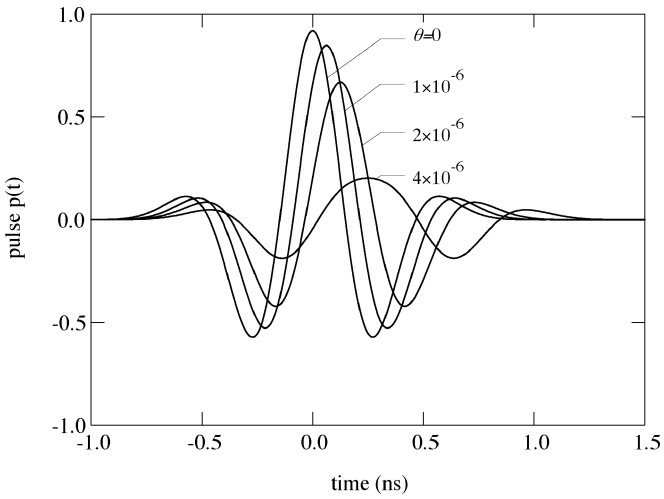

Fig. 1. Pulse $p(t)$ for some values of θ.

with $\gamma(t) = g(t) * g(-t)$. Note that $\gamma(t)$ is an even function, with a maximum in the origin, and $p(t)$ is the superposition of N time-shifted versions of $\gamma(t)$. Thus, for $\theta = 0$, we have $p(t) = \gamma(t)$ and (in the absence of noise) the maximum of $x(t)$ occurs exactly at $t = \tau$. On the contrary, for $\theta \neq 0$, the maximum is shifted from τ and (what is worse) its height is reduced. This increases the chance that the noise moves the peak of $x(t)$ further away from τ, thereby generating large estimation errors. Fig. 1 illustrates the shape of $p(t)$ for $N = 1250$, corresponding to an observation interval of 50 symbols, each of 25 frames. The frame period is $T_f = 100$ ns and $g(t)$ is the second derivative of a Gaussian function of 1-ns duration. It is seen that the height of the peak decreases as θ increases and the reduction becomes substantial for $\theta = 4 \times 10^{-6}$.

The above discussion indicates that frame-frequency synchronization in UWB systems is a difficult task, even with good oscillators. Some results on this problem are reported in [18], where a time-locked loop is used to acquire and track the incoming pulses. The channel has a dominant path and the pulses from that path are correlated with a template waveform timed by the voltage-controlled oscillator of the receiver. Unfortunately, this approach is not suitable with realistic multipath channels where there are hundreds of paths and a correlator matched to one of them would capture only a small fraction of the received power.

In the present paper, we take a different approach that exploits the whole received power. The idea is to transmit a sequence of pulses at frame rate and measure the period of the incoming waveform. The result can be used to trim the frequency of the receiver oscillator [19]. We focus on the estimation problem and we derive an algorithm that, in certain conditions, achieves the Cramer–Rao lower bound at high signal-to-noise ratio (SNR).

The rest of the paper is organized as follows. The next section describes the signal model and the estimation algorithm. The estimator performance is investigated in Section III, while simulations are discussed in Section IV. As we shall see, they validate the theory and indicate the degradations in estimation accuracy due to the interference from other UWB users. Some conclusions are drawn in Section V.

II. Frame-Frequency Estimation

A. Signal Model

For convenience, we assume that the transmitted signal is still periodic, as indicated in (3). The problem of the interference of its spectral lines on other systems operating in the same bandwidth deserves investigation, but is not addressed in the sequel. The propagation channel is modeled as a tapped-delay line with impulse response

$$c(t) = \sum_{l=1}^{L_p} \alpha_l \delta(t - \tau_l) \tag{8}$$

where L_p is the total number of paths, each with gain α_l and delay τ_l, and $\delta(t)$ is the Dirac delta function. Letting $h(t)$ be the convolution of $g(t)$ with $c(t)$ and the receive filter response, the overall channel output becomes

$$x(t) = \sum_{i=-\infty}^{\infty} h(t - iT_f) + n(t) \tag{9}$$

where $n(t)$ accounts for the thermal noise and the interference from the other users, and the summation limits have been extended to infinity to indicate that the pulse sequence is sufficiently long that it can be viewed as a periodic function over a suitable interval near the origin. Expressing this function as a Fourier series yields

$$\sum_{i=-\infty}^{\infty} h(t - iT_f) = \sum_{k=-\infty}^{\infty} H_k \mathrm{e}^{\frac{j2\pi kt}{T_f}} \tag{10}$$

in which

$$H_k = \frac{1}{T_f} H\left(\frac{k}{T_f}\right) \tag{11}$$

and $H(f)$ is the Fourier transform of $h(t)$. Then, bearing in mind that $H(f)$ is limited within some bandwidth $(0, B]$, we have

$$x(t) = \sum_{k=-\frac{L}{2}+1}^{\frac{L}{2}-1} H_k \mathrm{e}^{\frac{j2\pi kt}{T_f}} + n(t) \tag{12}$$

where $L/2 - 1 = \lfloor BT_f \rfloor$ and $\lfloor x \rfloor$ is the integer part of x.

We want to estimate $1/T_f$ from the samples of $x(t)$ taken at rate $1/T_s = L/T'_f$. For brevity, we let $x[i] = x(iT_s + t_0)$ and $n[i] = n(iT_s + t_0)$, where t_0 is an arbitrary constant. Then, exploiting (1) to express T_s in the form

$$T_s = \frac{T_f(1+\theta)}{L} \tag{13}$$

from (12) we get

$$x[i] = \sum_{k=-\frac{L}{2}+1}^{\frac{L}{2}-1} w_k \mathrm{e}^{\frac{j2\pi ki(1+\theta)}{L}} + n[i] \tag{14}$$

with

$$w_k = H_k \mathrm{e}^{\frac{j2\pi kt_0}{T_f}}. \tag{15}$$

Some unknown parameters appear in (14), the normalized drift θ and the coefficients $\{w_k\}$, collectively represented by the vector

$$\mathbf{w} = \left(w_{-\frac{L}{2}+1}, \ldots, w_0, \ldots, w_{\frac{L}{2}-1}\right)^{\mathrm{T}}. \tag{16}$$

In the following, we concentrate on θ because, as is seen from (1), the frequency offset between the transmitter and the receiver is proportional to θ

$$\frac{1}{T_f} - \frac{1}{T'_f} = \frac{\theta}{T'_f}. \tag{17}$$

In particular, we look for an algorithm that estimates θ based on the observation of $x[i]$ over an interval of M frames (LM samples), say $0 \le i \le LM - 1$.

B. Least-Squares Estimation

Assume that M can be factorized as $P \times Q$ and divide the observation interval into Q segments, each of LP samples. Also, collect the samples from the qth segment into a vector

$$\mathbf{x}_q = (x[qLP], x[qLP+1], \ldots, x[qLP+LP-1])^{\mathrm{T}}. \tag{18}$$

From (14), the mth component of $\mathbf{x}_q$ may be written as

$$[\mathbf{x}_q]_m = \sum_{k=-\frac{L}{2}+1}^{\frac{L}{2}-1} w_k \mathrm{e}^{j2\pi kqP\theta} \mathrm{e}^{\frac{j2\pi km(1+\theta)}{L}} + [\mathbf{n}_q]_m, \qquad m = 0, 1, \ldots, LP-1 \tag{19}$$

where $[\mathbf{n}_q]_m = n[m + qLP]$. Next, we make a temporary approximation to ease the derivation of the estimator. It consists of assuming LP as small compared to $1/|\theta|$, so that $\mathrm{e}^{j2\pi km\theta/L}$ can be set equal to unity in (19) for any $k \in [-L/2+1, L/2-1]$ and $m \in [0, LP-1]$. Note that this approximation is not used in Section III when dealing with the performance of the estimator. Equation (19) becomes

$$[\mathbf{x}_q]_m = \sum_{k=-\frac{L}{2}+1}^{\frac{L}{2}-1} w_k \mathrm{e}^{j2\pi kqP\theta} \mathrm{e}^{\frac{j2\pi km}{L}} + [\mathbf{n}_q]_m, \qquad m = 0, 1, \ldots, LP-1 \tag{20}$$

or more compactly

$$\mathbf{x}_q = \mathbf{E}\mathbf{D}_q(\theta)\mathbf{w} + \mathbf{n}_q, \qquad q = 0, 1, \ldots, Q-1 \tag{21}$$

where $\mathbf{E}$ is an $LP \times (L-1)$ matrix with entries

$$[\mathbf{E}]_{m,k} = \mathrm{e}^{\frac{j2\pi km}{L}} \tag{22}$$

$\mathbf{D}_q(\theta)$ is an $(L-1)\times(L-1)$ diagonal matrix

$$\mathbf{D}_q(\theta)=\operatorname{diag}\Big(\mathrm{e}^{j2\pi\left(-\frac{L}{2}+1\right)qP\theta},\ \mathrm{e}^{j2\pi\left(-\frac{L}{2}+2\right)qP\theta},\ldots,\mathrm{e}^{j2\pi\left(\frac{L}{2}-1\right)qP\theta}\Big) \quad (23)$$

and $\mathbf{w}$ is defined in (16). From now on, we assume $Q>1$ because, otherwise, the observation would reduce to $\mathbf{x}_0$, which is independent of the drift θ.

As $\mathbf{x}_q$ depends on both θ and $\mathbf{w}$, we aim at their joint estimation with the least squares (LS) method. To this end, we introduce trial values of θ and $\mathbf{w}$, say $\tilde{\theta}$ and $\tilde{\mathbf{w}}$, and minimize the cost function

$$J(\tilde{\theta},\tilde{\mathbf{w}})=\sum_{q=0}^{Q-1}\left\|\mathbf{x}_q-\mathbf{E}\mathbf{D}_q(\tilde{\theta})\tilde{\mathbf{w}}\right\|^2 \quad (24)$$

under the constraint $\tilde{w}_{-k}=\tilde{w}_k^*$. This constraint stems from fact that, as $h(t)$ is real-valued, its Fourier transform $H(f)$ is conjugate symmetric. From (11), it follows that $H_{-k}=H_k^*$ and, from (15), $w_{-k}=w_k^*$. The minimization of (24) is straightforward and is skipped for space limitations. The desired estimates are found to be

$$\hat{\theta}=\arg\max_{\tilde{\theta}}\left\{\left\|\mathbf{u}(\tilde{\theta})\right\|^2\right\} \quad (25)$$

$$\hat{\mathbf{w}}=\frac{1}{LPQ}\mathbf{u}(\hat{\theta}) \quad (26)$$

where

$$\mathbf{u}(\tilde{\theta})=\sum_{q=0}^{Q-1}\mathbf{D}_q^{\mathrm{H}}(\tilde{\theta})\mathbf{E}^{\mathrm{H}}\mathbf{x}_q \quad (27)$$

and the superscript "H" denotes Hermitian transposition. As is seen, the computation of $\hat{\theta}$ requires a grid search over the range of the possible values of θ. This is a consequence of the nonlinear dependence of $J(\tilde{\theta},\tilde{\mathbf{w}})$ on $\tilde{\theta}$, which prevents a closed-form solution.

A few remarks are in order.

1) Computation of $\|\mathbf{u}(\tilde{\theta})\|^2$: The following observations tend to ease the computational load. Rewrite (27) as

$$\mathbf{u}(\tilde{\theta})=\sum_{q=0}^{Q-1}\mathbf{D}_q^{\mathrm{H}}(\tilde{\theta})\mathbf{y}_q \quad (28)$$

with

$$\mathbf{y}_q=\mathbf{E}^{\mathrm{H}}\mathbf{x}_q. \quad (29)$$

Using (22) and performing some manipulations, the generic component of $\mathbf{y}_q$ may be expressed as

$$[\mathbf{y}_q]_k=\sum_{m=0}^{L-1}[\mathbf{z}_q]_m\mathrm{e}^{\frac{-j2\pi km}{L}},\qquad -\frac{L}{2}+1\le k\le\frac{L}{2}-1 \quad (30)$$

$$[\mathbf{z}_q]_m=\sum_{p=0}^{P-1}[\mathbf{x}_q]_{m+pL} \quad (31)$$

which says that $\mathbf{y}_q$ can be efficiently computed through L-point FFTs.

From (28), we have

$$\left\|\sum_{q=0}^{Q-1}\mathbf{D}_q^{\mathrm{H}}(\tilde{\theta})\mathbf{y}_q\right\|^2=\sum_{q=0}^{Q-1}\left\|\mathbf{D}_q^{\mathrm{H}}(\tilde{\theta})\mathbf{y}_q\right\|^2+2\Re e\left\{\sum_{q=0}^{Q-1}\sum_{m=q+1}^{Q-1}\mathbf{y}_q^{\mathrm{H}}\mathbf{D}_q(\tilde{\theta})\mathbf{D}_m^{\mathrm{H}}(\tilde{\theta})\mathbf{y}_m\right\} \quad (32)$$

where $\Re e\{x\}$ is the real part of x. Bearing in mind (23), it is easily checked that the first term on the right-hand side (RHS) of (32) is independent of $\tilde{\theta}$ and can be disregarded when maximizing $\|\mathbf{u}(\tilde{\theta})\|^2$. The second term can be rearranged as

$$2\Re e\left\{\sum_{q=1}^{Q-1}\sum_{k=-\frac{L}{2}+1}^{\frac{L}{2}-1}d_q[k]\mathrm{e}^{-j2\pi Pqk\tilde{\theta}}\right\} \quad (33)$$

with

$$d_q[k]=\sum_{m=0}^{Q-q-1}[\mathbf{y}_m]_k^*[\mathbf{y}_{m+q}]_k. \quad (34)$$

The inner summation in (33) may be computed through chirp Fourier-transform techniques (see [20, p. 151]) by varying $\tilde{\theta}$ on a grid with the desired resolution.

2) Factorization $P\times Q$: The choice of P and Q arises from a tradeoff between complexity and performance. In fact, the number of the Fourier transforms involved in the computation of $\mathbf{u}(\tilde{\theta})$ is proportional to Q, which suggests keeping Q as small as possible. On the other hand, reducing Q amounts to increasing P which, as we shall see in the next section, deteriorates the estimator performance.

III. Performance Evaluation

In this section, we compute the mean value and the variance of the estimator (25), and we provide the Cramer–Rao bound (CRB) for any unbiased estimator of θ. In dealing with these issues, we take a fixed channel and concentrate on the noise-induced fluctuations. To begin, we introduce the notation $\Lambda(\tilde{\theta})=\|\mathbf{u}(\tilde{\theta})\|^2$ and look for an explicit expression of $\hat{\theta}$, the maximizer of $\Lambda(\tilde{\theta})$. The main idea in doing so is that, with low noise levels, $\Lambda(\tilde{\theta})$ is expected to be a well-behaved function with a maximum close to θ. Thus, in a neighborhood of θ, we represent $\Lambda(\tilde{\theta})$ by a three-term Taylor series

$$\Lambda(\tilde{\theta})\cong\Lambda(\theta)+\Lambda'(\theta)(\tilde{\theta}-\theta)+\frac{1}{2}\Lambda''(\theta)(\tilde{\theta}-\theta)^2. \quad (35)$$

Setting to zero the derivative of $\Lambda(\tilde{\theta})$ and solving for $\tilde{\theta}$ yields

$$\hat{\theta}\cong\theta-\frac{\Lambda'(\theta)}{\Lambda''(\theta)}. \quad (36)$$

Dealing with this expression is still difficult because the second term in the RHS is a ratio of two random variables, which is hard to handle when computing the first and second moments of $\hat{\theta}$. On the other hand, in the absence of noise, we expect $\hat{\theta} = \theta$ and, correspondingly, $\Lambda'(\theta) = 0$ and $\Lambda''(\theta) < 0$. Thus, assuming a low noise level so that the fluctuations of $\Lambda''(\theta)$ are small, we replace $\Lambda''(\theta)$ by its expectation and rewrite (36) as

$$\hat{\theta} \cong \theta - \frac{\Lambda'(\theta)}{\mathbb{E}\{\Lambda''(\theta)\}} \tag{37}$$

from which the mean value and variance of $\hat{\theta}$ are derived in the form

$$\mathbb{E}\{\hat{\theta}\} = \theta - \frac{\mathbb{E}\{\Lambda'(\theta)\}}{\mathbb{E}\{\Lambda''(\theta)\}} \tag{38}$$

$$\mathbb{V}ar\{\hat{\theta}\} = \frac{\mathbb{E}\left\{[\Lambda'(\theta)]^2\right\}}{\left[\mathbb{E}\{\Lambda''(\theta)\}\right]^2}. \tag{39}$$

The expectations in (38) and (39) are computed in Appendix B under the assumption that the disturbance $n(t)$ in (9) can be modeled as a zero-mean Gaussian process with independent T_s-spaced samples. As mentioned in Section II, $n(t)$ is actually a mixture of thermal noise $n_{\mathrm{TH}}(t)$ and multiple-access interference (MAI) $n_{\mathrm{MAI}}(t)$. Accordingly, with a large number of interferers, the Gaussian approximation is well justified in view of the central-limit theorem. The independence of the samples is another question, however. If we take a receive filter with a rectangular transfer function over the bandwidth $|f| \leq 1/2T_s$ (as we do in Section IV), then it is easily checked that $n_{\mathrm{TH}}(t)$ does have independent samples. Unfortunately, the same property does not hold for $n_{\mathrm{MAI}}(t)$, so that our results are valid only in the absence of MAI.

Returning to the drift estimator and using formulas from Appendix B, it is found that

$$\mathbb{E}\{\hat{\theta}\} = \theta \tag{40}$$

$$\mathbb{V}ar\{\hat{\theta}\} = \frac{6}{(2\pi)^2 LP^3 Q(Q^2-1)} \times \frac{1}{\frac{1}{\sigma_n^2}\sum_{k=1}^{\frac{L}{2}-1} k^2 |H_k|^2 \left(\frac{\sin(\pi k P\theta)}{P\sin(\pi k\theta)}\right)^2} + O\left(\sigma_n^4\right) \tag{41}$$

where σ_n^2 is the variance of $n(t)$ and $O(\sigma_n^4)$ is proportional to σ_n^4. The following remarks are of interest.

1) Equation (40) says that the estimator is unbiased.
2) For an LP that is small compared with $1/|\theta|$, the ratio $\sin(\pi k P\theta)/[P\sin(\pi k\theta)]$ is approximately unity for any $k \in [1, L/2-1]$ and (41) becomes

$$\mathbb{V}ar\{\hat{\theta}\} = \frac{6}{(2\pi)^2 LP^3 Q(Q^2-1)} \times \frac{1}{\frac{1}{\sigma_n^2}\sum_{k=1}^{\frac{L}{2}-1} k^2 |H_k|^2} + O\left(\sigma_n^4\right). \tag{42}$$

Recalling that $PQ = M$ is the number of frames in the observation interval, we see that for $Q \gg 1$ and small noise levels (i.e., $O(\sigma_n^4)$ is negligible), the estimator accuracy increases with the cube of the observation interval. Even relatively small extensions of the observation interval correspond to significant improvements in estimation accuracy, a feature also encountered with carrier frequency-offset measurements ([15, p. 58]).

3) If LP is not small compared with $1/|\theta|$, the ratio $\sin(\pi k P\theta)/[P\sin(\pi k\theta)]$ is less than unity and the variance is greater than as expressed in (42). Thus, increasing P with a fixed M deteriorates the estimator accuracy.
4) The summation in (42) may be rearranged as a product

$$\frac{1}{\sigma_n^2}\sum_{k=1}^{\frac{L}{2}-1} k^2|H_k|^2 = \frac{\sum_{k=1}^{\frac{L}{2}-1}|H_k|^2}{\sigma_n^2} \times \frac{\sum_{k=1}^{\frac{L}{2}-1} k^2|H_k|^2}{\sum_{k=1}^{\frac{L}{2}-1}|H_k|^2}. \tag{43}$$

The first factor is proportional to the SNR, while the second may be viewed as the normalized mean-square bandwidth of the signal. Thus, the estimation accuracy improves not only with SNR (as expected) but also with the signal bandwidth. This is physically pleasing since the larger the bandwidth is, the sharper the pulses are, and the better they are "seen" in a background of noise. A similar conclusion holds true for clock recovery in narrowband transmissions ([15], p. 64).

5) Assuming a long observation interval ($M \gg 1$) and, once again, Gaussian and independent T_s-spaced samples of $n(t)$, it is found through lengthy calculations that the CRB for θ is

$$\mathrm{CRB} = \frac{6}{(2\pi)^2 LM^3} \frac{1}{\frac{1}{\sigma_n^2}\sum_{k=1}^{\frac{L}{2}-1} k^2|H_k|^2} \tag{44}$$

which coincides with the first term on the RHS of (42) for $Q \gg 1$. Thus, the CRB is achieved for an SNR $\gg 1$ and with parameter P sufficiently small.

IV. Simulation Results

A. Channel Model

The channel model is that indicated as CM3 by the IEEE 802.15.3a Channel Modeling Subcommittee for use in the evaluation of UWB physical-layer submissions [21]. Simulations with CM1 have also been run but are not reported as they are virtually identical to those with CM3. The channel impulse response is represented by

$$c(t) = X\sum_{l=1}^{L_c}\sum_{k=1}^{L_r} \alpha_{k,l}\delta(t - T_l - \tau_{k,l}) \tag{45}$$

where X is the attenuation due to shadowing, $\alpha_{k,l}$ is the gain coefficient of the kth ray in the lth cluster, T_l is the arrival time of the lth cluster, and $\tau_{k,l}$ is the delay of the kth ray in the lth cluster relative to the beginning of the cluster. The attenuation has a log-normal distribution, i.e., $20\log_{10} X \in \mathcal{N}(0, \sigma_x^2)$. The

cluster arrival times are Poisson distributed with rate Λ and the rays within a cluster also have Poisson arrivals with rate λ. The gain coefficients are defined as $\alpha_{k,l} = p_{k,l}\beta_{k,l}$, where $p_{k,l}$ takes values ± 1 with the same probability and accounts for signal inversions due to reflections, while $\beta_{k,l}$ are independent log-normally distributed random variables, i.e.,

$$20\log_{10}\beta_{k,l} \in \mathcal{N}\left(\mu_{k,l}, \sigma_1^2 + \sigma_2^2\right). \quad (46)$$

Parameter $\mu_{k,l}$, reflecting the power decay over the clusters and within a given cluster, is given by

$$\mu_{k,l} = \frac{10\ln\Omega_0 - \frac{10T_l}{\Gamma} - \frac{10\tau_{k,l}}{\gamma}}{\ln 10} - \frac{\left(\sigma_1^2 + \sigma_2^2\right)\ln 10}{20} \quad (47)$$

where Γ and γ are the cluster decay factor and the ray decay factor, respectively, whereas Ω_0 is the mean energy of the first ray in the first cluster.

In the simulations, X is set equal to 1 and Ω_0 is chosen so as to normalize to unity the total energy of the gains $\{\alpha_{k,l}\}$. This is easily accomplished bearing in mind that $\mathbb{E}\{\alpha_{k,l}^2\} = \Omega_0 \mathrm{e}^{-T_l/\Gamma}\mathrm{e}^{-\tau_{k,l}/\gamma}$. The normalization implies that the interferers have the same power. The following parameters values have been chosen: $\Lambda = 0.0667$ ns^{-1}, $\lambda = 2.1$ ns^{-1}, $\Gamma = 14.00$, $\gamma = 7.9$, $\sigma_1 = \sigma_2 = 3.39$ (dB), $\sigma_x = 3$ (dB). They correspond to a 4–10 m channel with non-line-of-sight (LOS) propagation [21] and a typical response duration of 60–70 ns.

B. Signal and Interference

We assume that K_u users are simultaneously active in the environment, each "seeing" his own channel that is generated with the statistics described above. The first user transmits the synchronizing signal (3), while the others are viewed as the interferers and transmit antipodal pulse-amplitude-modulation (PAM) symbols. The signal generated by the kth user is modeled as

$$s^{(k)}(t) = \sum_{i=-\infty}^{\infty}\sum_{j=0}^{N_f-1} a_i^{(k)} g\left(t - iN_fT_f - jT_f - c_j^{(k)}T_c - \tau^{(k)}\right), \quad k = 2, \ldots, K_u \quad (48)$$

In this formula, $a_i^{(k)}$ are information bits taking values ± 1 with equal probability and $g(t)$ represents the elementary pulse, which is shaped as the second derivative of a Gaussian function with a width of 1 ns. The frame period T_f is 100 ns and the number of frames per symbol N_f is 25. Parameter T_c is the chip duration, equal to 1 ns, and the sequence $\{c_j^{(k)}\}$ is the user's time-hopping code. Its elements are integers that are randomly chosen in the range $0 \le c_j^{(k)} \le 39$ (independently from one user to the other). Finally, the delay $\tau^{(k)}$ accounts for the asynchronism of the users and is uniformly distributed in the range $0 \le \tau^{(k)} < N_fT_f$.

The receive filter has a rectangular transfer function over $\pm B$ and the sampling frequency $1/T_s$ is $2B$. In the simulations, B is either 4, 2, or 1 GHz and ideal sampling is assumed (infinite resolution). As mentioned in Section II, the disturbance $n(t)$ in (9) is a mixture of thermal noise and multiple-access interference. The former is a Gaussian process with a two-sided power spectral density $N_0/2$ over the filter bandwidth.

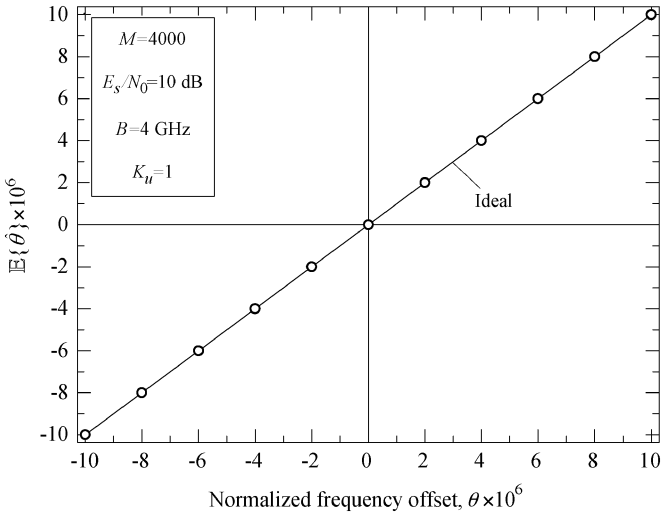

Fig. 2. Expectation of the estimate as a function of θ.

Bearing in mind that the channel response has no dc component ($H_0 = 0$), the power of the synchronizing signal is [see (12)]

$$P_s = 2\sum_{k=1}^{\frac{L}{2}-1} |H_k|^2. \quad (49)$$

The signal energy over N_f frames (a symbol interval) is $E_s = P_sN_fT_f$. In the sequel, the performance of the estimator is expressed as a function of E_s/N_0 for a given number K_u of active users.

C. Simulations

Fig. 2 shows the expectation $\mathbb{E}\{\hat{\theta}\}$ as a function of θ with an observation interval of 4000 frames. There is no MAI ($K_u = 1$) and $E_s/N_0 = 10$ dB. Marks represent simulations while the solid line corresponds to the ideal case $\mathbb{E}\{\hat{\theta}\} = \theta$. The results confirm that the estimator is unbiased. Identical conclusions hold true in the presence of MAI.

Figs. 3–5 illustrate the root mean-square error (RMSE) $\sigma_\theta = \sqrt{\mathbb{V}ar\{\hat{\theta}\}}$ as a function of E_s/N_0 for $\theta = 10^{-5}$. The observation interval is 4000 frames, but a different factorization $M = P \times Q$ is used in the figures. The bandwidth of the receive filter is 4 GHz, which corresponds to $L = 802$. The CRB is shown as a reference and the theoretical curves are computed from (41). With a single user, it is seen that the CRB is practically achieved at high SNR in Fig. 3, where the parameter P has the lowest value. In the other two figures, the loss from the CRB is apparent and grows larger as P increases. As expected, in the presence of MAI, the curves exhibit a floor. The RMSE in Fig. 5 shows a deviation from the theory at low E_s/N_0 due to the insurgence of large estimation errors. This phenomenon is typical of nonlinear estimators (see [22, p. 616]) and is also visible in Figs. 3 and 4 at lower values of E_s/N_0.

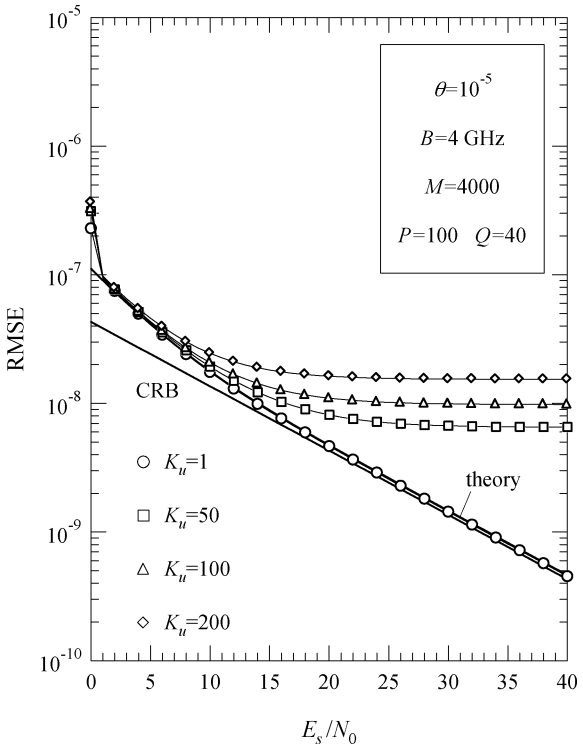

Fig. 3. RMSE versus E_s/N_0 for $P = 100$ and $Q = 40$.

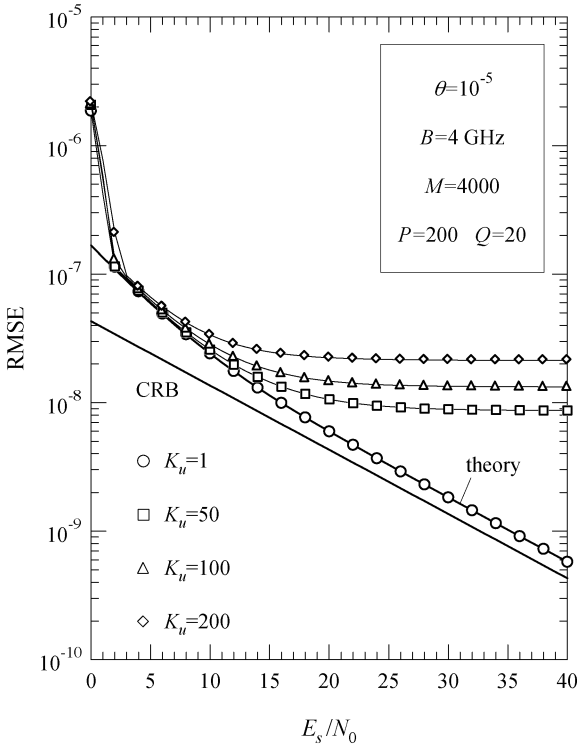

Fig. 4. RMSE versus E_s/N_0 for $P = 200$ and $Q = 20$.

The role of the filter bandwidth B is shown in Fig. 6 in the absence of MAI. The CRB is computed for $B = 4$ GHz. As expected, the estimation accuracy worsens as the filter bandwidth is squeezed. Actually, the degradation is limited in passing from 4 to 2 GHz, but it becomes substantial for $B = 1$ GHz.

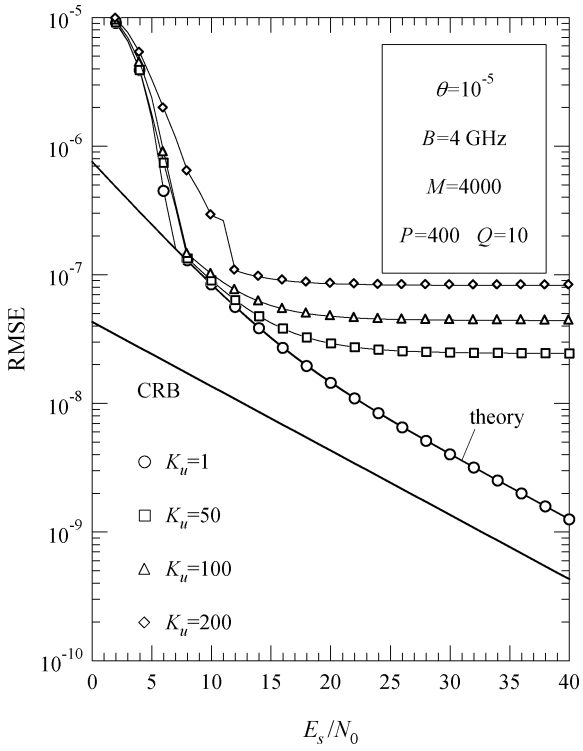

Fig. 5. RMSE versus E_s/N_0 for $P = 400$ and $Q = 10$.

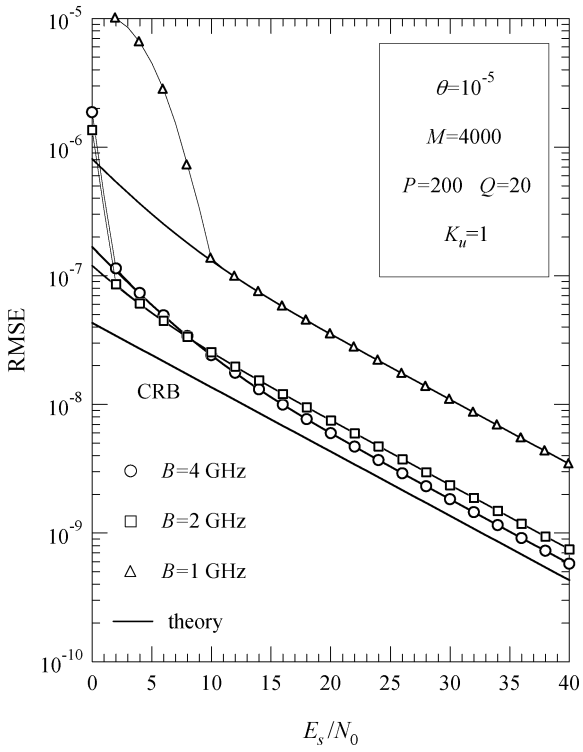

Fig. 6. RMSE versus E_s/N_0 for $K_u = 1$ and various B's.

In Fig. 7 the filter bandwidth is 1 GHz, but the observation interval has been doubled to 8000 frames. For $K_u = 1$ and $E_s/N_0 \gg 1$, the RMSE is reduced by a factor around $\sqrt{8}$ with respect to the corresponding values in Fig. 6, which is in keeping with (41).

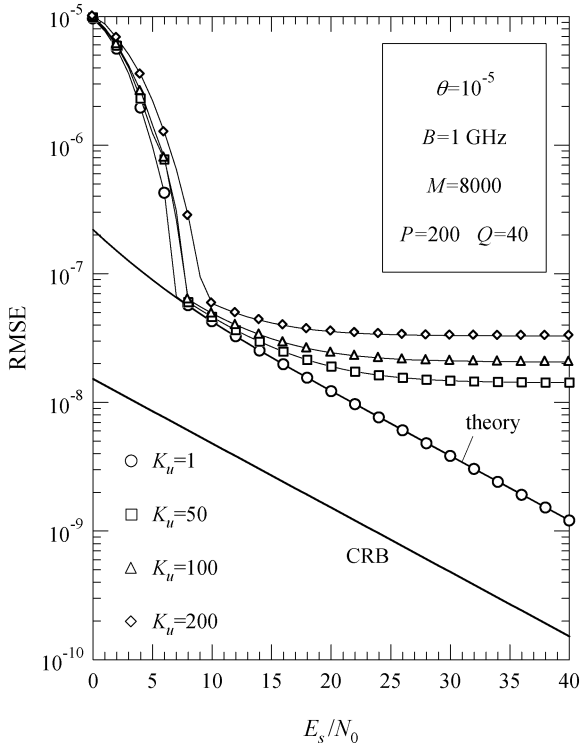

Fig. 7. RMSE versus E_s/N_0 for $M = 8000$ and $B = 1$ GHz.

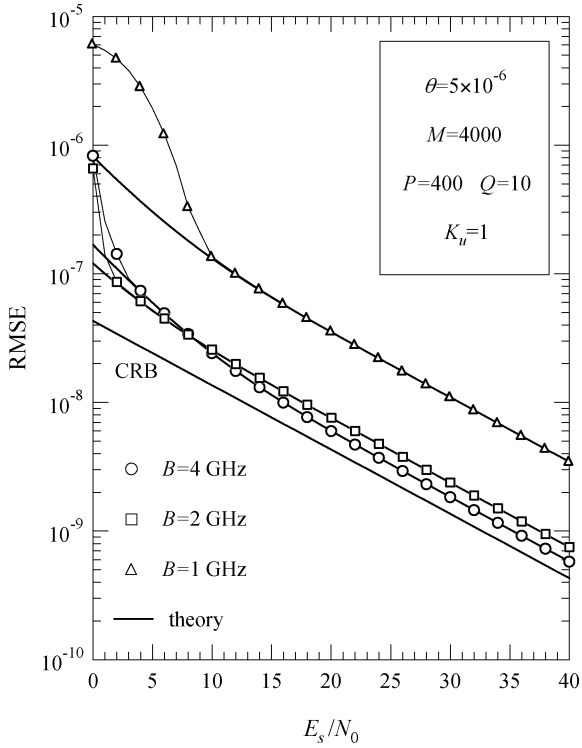

Fig. 8. RMSE versus E_s/N_0 for $K_u = 1$ and various B's.

In Fig. 8, the observation interval is brought back to 4000 frames, while θ is set at 5×10^{-6} (instead of 10^{-5} as in the previous figures). This corresponds to a scenario with more stable oscillators. It is seen that the estimator performance is virtually the same as in Fig. 6, but the advantage is that Q is 10 instead of 20, which implies a reduced computational load.

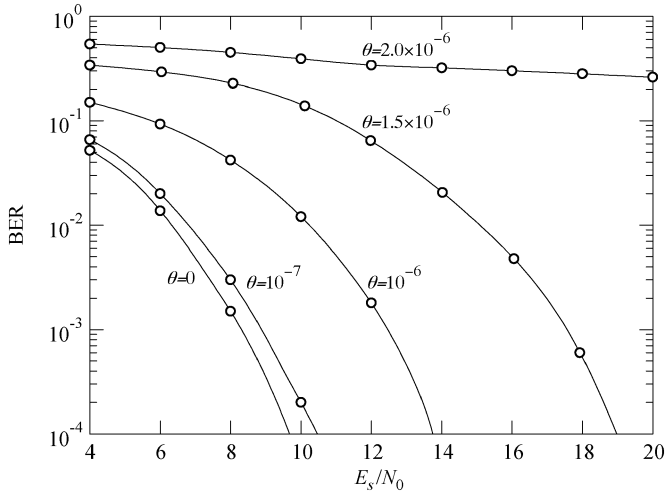

Fig. 9. BER performance for some values of θ.

A natural question at this stage is about the order of magnitude of the RMSE that must be guaranteed in a practical situation. To address this problem, we have simulated a correlation receiver in which the channel response is estimated in the presence of drift. The estimation method is described in [8] and is summarized here for convenience. The received waveform is given in (9) and the goal is to estimate $h(t)$ from the observation of $x(t)$ over an interval of M frames. In doing so, we ignore the mismatch between T_f' and T_f and we model the deterministic component in (9) as

$$\sum_{i=-\infty}^{\infty} \tilde{h}\left(t - iT_f'\right) \tag{50}$$

where $\tilde{h}(t)$ represents a hypothetical realization of $h(t)$. The channel response is estimated by minimizing the cost function

$$\int_0^{MT_f'} \left[x(t) - \sum_{i=-\infty}^{\infty} \tilde{h}\left(t - iT_f'\right)\right]^2 dt \tag{51}$$

with respect to $\tilde{h}(t)$. Once the channel estimate $\hat{h}(t)$ is available, the data transmission begins with a binary PAM modulation format and $\hat{h}(t)$ is used as a template waveform in the correlation receiver.

In the simulations, M is set equal to 1250 (corresponding to an observation of 50 symbols) and ideal symbol synchronization is assumed. In particular, the start of the first frame is perfectly known. Fig. 9 illustrates the bit error rate (BER) of the receiver for some values of θ. At a BER equal to 10^{-4}, the loss incurred with $\theta = 10^{-6}$ is 4 dB and with $\theta = 1.5 \times 10^{-6}$ is 9.5 dB. We see that with the selected parameters, the RMSE should be around 10^{-7} to make the drift effects negligible.

V. Conclusion

We have investigated the frame-frequency estimation problem in UWB systems. The proposed solution is based on the transmission of a periodic pulse sequence at the frame frequency. The samples of the received waveform are used to

compute a cost function whose maximum gives the desired estimate. The performance of the estimator has been assessed analytically and, under certain conditions, it has been found close to the Cramer–Rao lower bound. Simulations have been run to check the validity of the theoretical development and to assess the impact of the multiple-access interference. Finally, a correlation receiver has been simulated wherein the channel response is estimated in the presence of a frame-frequency offset. It has been found that the offset must be kept within about 10^{-7} to avoid severe BER degradations. This accuracy can be achieved by the proposed frequency estimator.

APPENDIX A

In this appendix, we derive the maximum likelihood estimator of the delay τ in the model (4). As the noise is white and Gaussian by assumption, the estimator minimizes the function

$$J(\tilde{\tau}) = \int_{-\infty}^{+\infty} \left[r(t) - \sum_{i=0}^{N-1} g\left(t - iT_f' - \tilde{\tau}\right) \right]^2 dt. \tag{52}$$

Expanding the square in the integrand and dropping quantities independent of $\tilde{\tau}$, after some algebraic manipulations, it is found that minimizing (52) amounts to maximizing

$$F(\tilde{\tau}) = \int_{-\infty}^{+\infty} r_{\text{fold}}(t) g(t - \tilde{\tau}) dt \tag{53}$$

where $r_{\text{fold}}(t)$ is defined in (5). As the integral in (53) is the response of the filter $g(-t)$ to the excitation $r_{\text{fold}}(t)$ at time $t = \tilde{\tau}$, the estimator operation amounts to looking for the maximum of the filter output.

To compute the noiseless component of $x(t)$, say $p(t - \tau)$, we insert (3) and (4) into (5), setting $v(t) = 0$. As a result we get

$$p(t - \tau) = \frac{1}{N} \sum_{i=0}^{N-1} \sum_{j=0}^{N-1} g\left[t + i\theta T_f + (i - j)T_f - \tau\right] \tag{54}$$

where the relation $T_f' = (1 + \theta)T_f$ has been used. Next, bearing in mind that $g(t)$ is very short compared with T_f and $\theta \ll 1$, from (54) we see that $p(t - \tau)$ has several peaks spaced T_f seconds apart in time. The highest peak is located around $t = \tau$ and is expressed by

$$\frac{1}{N} \sum_{i=0}^{N-1} \gamma(t + i\theta T_f - \tau). \tag{55}$$

APPENDIX B

In this appendix, we compute the expectations $\mathbb{E}\{\Lambda'(\theta)\}$, $\mathbb{E}\{\Lambda''(\theta)\}$, and $\mathbb{E}\{[\Lambda'(\theta)]^2\}$ appearing in (37)–(39). Letting $\Lambda(\theta) = \|\mathbf{u}(\theta)\|^2$ and

$$\mathbf{v}_q(\theta) = \mathbf{D}_q^{\mathrm{H}}(\theta)\mathbf{y}_q \tag{56}$$

from (28), we have

$$\Lambda' = j2\pi P \sum_{p=0}^{Q-1} \sum_{q=0}^{Q-1} (p - q)\mathbf{v}_p^{\mathrm{H}} \mathbf{A} \mathbf{v}_q \tag{57}$$

$$\Lambda'' = -(2\pi P)^2 \sum_{p=0}^{Q-1} \sum_{q=0}^{Q-1} (p - q)^2 \mathbf{v}_p^{\mathrm{H}} \mathbf{A}^2 \mathbf{v}_q \tag{58}$$

$$[\Lambda']^2 = -(2\pi P)^2 \sum_{p_1=0}^{Q-1} \sum_{q_1=0}^{Q-1} \sum_{p_2=0}^{Q-1} \sum_{q_2=0}^{Q-1} (p_1 - q_1)(p_2 - q_2) \times \mathbf{v}_{p_1}^{\mathrm{H}} \mathbf{A} \mathbf{v}_{q_1} \mathbf{v}_{p_2}^{\mathrm{H}} \mathbf{A} \mathbf{v}_{q_2} \tag{59}$$

where $\mathbf{A} = \operatorname{diag}\{-L/2 + 1, -L/2 + 2, \ldots, L/2 - 1\}$ and the dependence on θ is understood throughout. Collecting (21), (29), and (56) yields

$$\mathbf{v}_p = \mathbf{D}_p^{\mathrm{H}} \mathbf{E}^{\mathrm{H}} \mathbf{F} \mathbf{D}_p \mathbf{w} + \mathbf{m}_p \tag{60}$$

where

$$\mathbf{m}_p = \mathbf{D}_p^{\mathrm{H}} \mathbf{E}^{\mathrm{H}} \mathbf{n}_p \tag{61}$$

and $\mathbf{F}$ is an $LP \times (L - 1)$ matrix with elements

$$[\mathbf{F}]_{p,q} = \mathrm{e}^{j2\pi pq(1+\theta)}.$$

The statistics of $\mathbf{m}_p$ are of crucial importance. Assuming that $\mathbf{n}_p$ can be modeled as a Gaussian vector with zero-mean independent components, each of variance σ_n^2, and that $\mathbf{n}_p$ and $\mathbf{n}_q$ are independent for $p \neq q$, then the following can be shown: 1) $\mathbf{m}_p$ has zero-mean components, each with variance $PL\sigma_n^2$; 2) $\mathbf{m}_p$ and $\mathbf{m}_q$ are independent for $p \neq q$. Also, calling $[\mathbf{m}_p]_k$ the kth component of $\mathbf{m}_p$, it is found that

$$\mathbb{E}\left\{ [\mathbf{m}_p]_{k_1} [\mathbf{m}_p]_{k_2}^* \right\} = PL\sigma_n^2 \delta_{k_1, k_2} \tag{62}$$

$$\mathbb{E}\left\{ [\mathbf{m}_p]_{k_1} [\mathbf{m}_p]_{k_2} \right\} = PL\sigma_n^2 \delta_{k_1, -k_2} \tag{63}$$

where $\delta_{l,m}$ equals unity for $l = m$, and is zero otherwise.

Making use of these facts and performing some boring calculations leads to

$$\mathbb{E}\{\Lambda'(\theta)\} = 0 \tag{64}$$

$$\mathbb{E}\{\Lambda''(\theta)\} = -\frac{1}{3}(2\pi P)^2 Q^2 (Q^2 - 1) L^2 \times \sum_{k=1}^{\frac{L}{2}-1} k^2 |H_k|^2 \left(\frac{\sin(\pi k P \theta)}{\sin(\pi k \theta)} \right)^2 \tag{65}$$

$$\mathbb{E}\left\{ [\Lambda'(\theta)]^2 \right\} = \frac{2}{3}\sigma_n^2 (2\pi)^2 P^3 Q^3 (Q^2 - 1) L^3 \times \sum_{k=1}^{\frac{L}{2}-1} k^2 |H_k|^2 \left(\frac{\sin(\pi k P \theta)}{\sin(\pi k \theta)} \right)^2 + \frac{1}{36}\sigma_n^4 (2\pi P)^2 P^2 Q^2 (Q^2 - 1) \times L^3 (L - 1)(L - 2). \tag{66}$$

REFERENCES

[1] M. Z. Win and R. A. Scholtz, "Impulse radio: How it works," *IEEE Commun. Lett.*, vol. 2, no. 2, pp. 36–38, Feb. 1998.

[2] ——, "Ultra-wide bandwidth time-hopping spread-spectrum impulse radio for wireless multiple access communications," *IEEE Trans. Commun.*, vol. 48, no. 4, pp. 679–691, Apr. 2000.

[3] W. M. Lovelace and J. K. Townsend, "The effect of timing jitter and tracking on the performance of impulse radio," *IEEE J. Sel. Areas Commun.*, vol. 20, no. 9, pp. 1646–1651, Dec. 2002.

[4] V. Lottici, A. N. D'Andrea, and U. Mengali, "Channel estimation for ultra-wideband communications," *IEEE J. Sel. Areas Commun.*, vol. 20, no. 9, pp. 1638–1645, Dec. 2002.

[5] W. Namgoong, "A channelized digital ultrawideband receiver," *IEEE Trans. Wireless Commun.*, vol. 2, no. 3, pp. 502–510, May 2003.

[6] I. O'Donnel, M. S. W. Chen, S. B. T. Wang, and R. W. Brodersen, "An integrated, low-power, ultra-wideband transceiver architecture for low-rate indoor wireless systems," presented at the IEEE CAS Workshop Wireless Communications and Networking, Pasadena, CA, Sep. 2002.

[7] J. D. Choi and W. E. Stark, "Performance of ultra-wideband communications with suboptimal receivers in multipath channels," *IEEE J. Sel. Areas Commun.*, vol. 20, no. 9, pp. 1754–1766, Dec. 2002.

[8] C. Carbonelli, U. Mengali, and U. Mitra, "Synchronization and channel estimation for UWB signals," in *Proc. Global Telecommunications (GLOBECOM)*, San Francisco, CA, Dec 1–5, 2003, pp. 764–768.

[9] S. Franz and U. Mitra, "On optimal data detection for UWB transmitted reference systems," in *Proc. Global Telecommunications (GLOBECOM)*, San Francisco, CA, Dec. 1–5, 2003, pp. 744–748.

[10] L. Yang and G. B. Giannakis, "Optimal pilot waveform assisted modulation for ultra-wideband communications," *IEEE Trans. Wireless Commun.*, vol. 3, no. 4, pp. 1236–1249, Jul. 2004.

[11] A. Taha and K. M. Chugg, "On designing the optimal template waveform for UWB impulse radio in the presence of multipath," in *Proc. IEEE Conf. Ultra Wideband Systems and Techniques*, Baltimore, MD, 2002, pp. 41–45.

[12] H. Sheng, P. Orlik, A. M. Haimovich, L. J. Cimini, and J. Zhang, "On the spectral and power requirements for ultra-wideband transmission," in *Proc. Int. Conf. Communications (ICC)*, Anchorage, AL, May 11–15, 2003, pp. 738–742.

[13] J. Bellorado, S. Ghassemzadeh, L. Greenstein, T. Sveinsson, and V. Tarokh, "Coexistence of ultra-wideband systems with IEEE-802.11a wireless LANs," in *Proc. Global Telecommunications (GLOBECOM)*, San Francisco, CA, Dec. 1–5, 2003, pp. 410–414.

[14] C. Carbonelli, S. Vedantam, and U. Mitra, "Sparse channel estimation with zero tap detection," in *Proc. Int. Conf. Communications (ICC)*, Paris, France, Jun. 20–24, 2003, pp. 3173–3177.

[15] U. Mengali and A. N. D'Andrea, *Synchronization Techniques for Digital Receivers*. New York: Plenum, 1997.

[16] H. Meyr, M. Moeneclaey, and S. A. Fechtel, *Digital Communications Receivers*. New York: Wiley, 1998.

[17] M. Z. Win and R. A. Scholtz, "Characterization of ultra-wide bandwidth wireless communications channels: A communication theoretic view," *IEEE J. Sel. Areas Commun.*, vol. 20, no. 9, pp. 1613–1627, Dec. 2002.

[18] C.-C. Chui and R. A. Scholtz, "Optimizing tracking loops for UWB monocycles," in *Proc. Global Telecommunications (GLOBECOM)*, San Francisco, CA, Dec. 2003, pp. 425–430.

[19] Q. Huang and P. Basedau, "A 200 micro A, 78 mhz cmos crystal oscillator digitally trimmable to 0.3 ppm," in *Int. Symp. Low Power Electronics and Design*, Montery, CA, Aug. 1996, pp. 305–308.

[20] B. Porat, *A course in Digital Signal Processing*. New York: Wiley, 1997.

[21] IEEE P802.15 Working Group for Wireless Personal Area Network, *Channel model subcommittee report final*, Tech. Rep., Dec. 2002.

[22] J. Wozencraft and I. Jacobs, *Principles of Communication Engineering*. New York: Wiley, 1965.

Antonio A. D'Amico received the Dr. Eng. degree in electronic engineering in 1992 and the Ph.D. degree in 1997, both from the University of Pisa, Pisa, Italy.

He is currently a Research Fellow in the Department of Information Engineering of the University of Pisa. His research interests are in digital-communication theory, with emphasis on synchronization algorithms, channel estimation, and detection techniques.

Umberto Mengali (M'69–SM'85–F'90–LF'03) received the "Laurea" degree in electrical engineering in 1961 from the University of Pisa, Pisa, Italy. In 1971, he received the Libera Docenza in Telecommunications from the Italian Education Ministry.

Since 1963, he has been with the Department of Information Engineering, University of Pisa, where he is a Professor of Telecommunications. In 1994, he was a Visiting Professor at the University of Canterbury, New Zealand, as an Erskine Fellow. His research interests are in digital communications and communication theory, with emphasis on synchronization methods and modulation techniques. He has coauthored the book *Synchronization Techniques for Digital Receivers* (New York: Plenum, 1997). He was an Editor of the *European Transactions on Telecommunications* from 1997 to 2000.

Prof. Mengali is a Member of the Communication Theory Committee and was an Editor of the IEEE TRANSACTIONS ON COMMUNICATIONS from 1985 to 1991. He has served on the Technical Program Committees of several international conferences and was Technical Co-chair of the 2004 International Symposium on Information Theory and Applications (ISITA).